Early Functional Connectome Integrity and 1-Year Recovery in Comatose Survivors of Cardiac Arrest[1]

Haris I. Sair, MD
Yousef Hannawi, MD[2]
Shanshan Li, PhD
Joshua Kornbluth, MD
Athena Demertzi, PhD
Carol Di Perri, MD, PhD
Russell Chabanne, MD
Betty Jean, MD
Habib Benali, PhD
Vincent Perlbarg, PhD
James Pekar, PhD
Charles-Edouard Luyt, MD, PhD
Damien Galanaud, MD, PhD
Lionel Velly, MD
Louis Puybasset, MD, PhD
Steven Laureys, MD, PhD
Brian Caffo, PhD
Robert D. Stevens, MD
For the Neuroimaging for Coma Emergence and Recovery (NICER) Consortium

[1] From the Departments of Radiology and Radiological Science (H.I.S., R.D.S.), Anesthesiology and Critical Care Medicine (Y.H., R.D.S.), Neurology (Y.H., R.D.S.), and Neurosurgery (R.D.S.), Johns Hopkins University School of Medicine, 600 N Wolfe St, Phipps 455, Baltimore, MD 21287; Department of Biostatistics, Indiana University Fairbanks School of Public Health, Indianapolis, Ind (S.L.); Department of Neurology, Tufts University School of Medicine, Boston, Mass (J.K.); Institut du Cerveau et de la Moelle Épinière, Groupe Hospitalier Pitié-Salpêtrière, Paris, France (A.D.); Coma Science Group and Department of Neurology, University of Liège, Liège, Belgium (C.D.P., S.L.); Departments of Anesthesia Resuscitation (R.C.) and Neuroradiology (B.J.), Centre Hospitalier Universitaire, Clermont-Ferrand, France; Functional Imaging Laboratory U678, Faculté de Médecine Pierre et Marie Curie, Paris, France (H.B., V.P.); F.M. Kirby Center for Functional Brain Imaging, Kennedy Krieger Institute, Baltimore, Md (J.P.); Medical Resuscitation Service (C.E.L.), Department of Neuroradiology (D.G.), and Neurosurgical Resuscitation Service (L.V., L.P.), Groupe Hospitalier Pitié-Salpêtrière, Assistance Publique-Hôpitaux de Paris, and Université Pierre et Marie Curie, Paris, France; and Department of Biostatistics, Johns Hopkins Bloomberg School of Public Health, Baltimore, Md (B.C.). Received September 16, 2016; revision requested November 28; revision received June 21, 2017; accepted July 10; final version accepted July 28. **Address correspondence to** R.D.S. (e-mail: *rstevens@jhmi.edu*).

[2] **Current address:** Department of Neurology, The Ohio State University, Columbus, Ohio.

Purpose: To assess whether early brain functional connectivity is associated with functional recovery 1 year after cardiac arrest (CA).

Materials and Methods: Enrolled in this prospective multicenter cohort were 46 patients who were comatose after CA. Principal outcome was cerebral performance category at 12 months, with favorable outcome (FO) defined as cerebral performance category 1 or 2. All participants underwent multiparametric structural and functional magnetic resonance (MR) imaging less than 4 weeks after CA. Within- and between-network connectivity was measured in dorsal attention network (DAN), default-mode network (DMN), salience network (SN), and executive control network (ECN) by using seed-based analysis of resting-state functional MR imaging data. Structural changes identified with fluid-attenuated inversion recovery and diffusion-weighted imaging sequences were analyzed by using validated morphologic scales. The association between connectivity measures, structural changes, and the principal outcome was explored with multivariable modeling.

Results: Patients underwent MR imaging a mean 12.6 days ± 5.6 (standard deviation) after CA. At 12 months, 11 patients had an FO. Patients with FO had higher within-DMN connectivity and greater anticorrelation between SN and DMN and between SN and ECN compared with patients with unfavorable outcome, an effect that was maintained after multivariable adjustment. Anticorrelation of SN-DMN predicted outcomes with higher accuracy than fluid-attenuated inversion recovery or diffusion-weighted imaging scores (area under the receiver operating characteristic curves, respectively, 0.88, 0.74, and 0.71).

Conclusion: MR imaging–based measures of cerebral functional network connectivity obtained in the acute phase of CA were independently associated with FO at 1 year, warranting validation as early markers of long-term recovery potential in patients with anoxic-ischemic encephalopathy.

Cardiac arrest (CA) is reported in 535 000 individuals in the United States annually and is a leading cause of death (1), while survivors suffer from varying degrees of anoxic brain injury with long-term functional disability and cognitive impairment (2). A challenge in the care of patients after CA is that individuals with similarly manifesting characteristics may have markedly different outcomes, ranging from death or states of chronically depressed consciousness to complete recovery. Recent studies (3,4) indicate that the accuracy of outcome classification can be enhanced with advanced electroencephalography or evoked-potential analysis. However, current prognostic models fail to predict coma emergence and cognitive recovery with a degree of accuracy and reproducibility that would be useful at single-subject level (5). Moreover, the validity of existing prognostic approaches is reduced in patients who received therapeutic temperature management (4,6,7).

It has been proposed (5) that predictive accuracy could be enhanced with methods that examine underlying biologic or neurophysiological differences after CA. Detailed characterization of post-CA tissue changes can be realized with diffusion-weighted brain magnetic resonance (MR) imaging (8), and both global or regional patterns of restricted diffusion have been linked to clinical outcome (9,10). In a study (11) that used quantitative diffusion-tensor imaging in the acute post-CA setting, a prediction model that integrated diffusion-tensor imaging measures of corpus callosum integrity classified long-term outcomes with greater accuracy than a clinical prediction model. Moreover, decreased functional activity and loss of connectivity within certain brain regions are consistently observed in the chronic phases that follow various brain injures (12). These findings suggest that recovery after CA might be determined, at least in part, by a pathophysiologic substrate of anatomic and functional disconnection. To study these patients who were comatose and unable to engage in a specified activity, we used a multimodal MR imaging sequence that included resting-state functional MR imaging. Resting-state functional MR imaging indicates that the brain is organized in discrete large-scale intrinsic functional networks with distributed topologic features that are congruent with known sensorimotor and cognitive systems (13–16). Resting-state networks are dynamic systems that change throughout the lifespan and in relation to physiologic processes such as learning and sleep (17). In addition, network-based conceptual models suggest a systems-level approach to understand and treat neurodevelopmental, neurologic, and psychiatric disorders (16,18,19). We hypothesized that connectivity within and between four canonical resting-state networks would be altered in the acute phase after CA, and that the magnitude of connectivity disruption would be linked to 1-year functional outcome. The purpose of this study was to assess whether early brain functional connectivity is associated with functional recovery 1 year after CA.

Advances in Knowledge

- In comatose patients evaluated early (mean, 12.6 days; range, 6–28 days) after cardiac arrest (CA), resting-state functional MR imaging identified specific patterns of connectivity within and between higher order intrinsic brain networks that were markedly reduced when compared with healthy control participants.
- Patients with favorable 1-year functional outcome had greater preservation of connectivity within the default-mode network (DMN; $P = .002$), as well as higher levels of connectivity between the salience network and the DMN ($P < .001$), when compared with patients with unfavorable outcome.
- Functional connectivity changes between networks discriminated between outcome categories with greater accuracy than any of the tested MR imaging structural measures (*c*-statistic: 0.88, 0.73, and 0.71, respectively, for default mode-salience network connectivity, diffusion-weighted imaging score, and fluid-attenuated inversion recovery score).

Implication for Patient Care

- MR imaging performed in the acute phase after CA indicates that network functional connectivity measures increase the accuracy of outcome prediction, which suggests a novel prognostic biomarker.

Materials and Methods

Participants

Study participants were identified retrospectively within a prospective observational cohort of patients admitted to the intensive care unit with severe brain injury at three centers (Groupe Hospitalier Pitié-Salpêtrière, Paris, France; Centre Hospitalier Universitaire de Clermont Ferrand, Clermont-Ferrand, France;

https://doi.org/10.1148/radiol.2017162161

Content code: NR

Radiology 2018; 287:247–255

Abbreviations:
CA = cardiac arrest
DAN = dorsal attention network
DMN = default-mode network
DWI = diffusion-weighted imaging
ECN = executive control network
FLAIR = fluid-attenuated inversion recovery
FO = favorable outcome
SN = salience network

Author contributions:
Guarantors of integrity of entire study, H.I.S., H.B., L.V., R.D.S.; study concepts/study design or data acquisition or data analysis/interpretation, all authors; manuscript drafting or manuscript revision for important intellectual content, all authors; approval of final version of submitted manuscript, all authors; agrees to ensure any questions related to the work are appropriately resolved, all authors; literature research, H.I.S., Y.H., J.K., C.D.P., R.D.S.; clinical studies, H.I.S., Y.H., J.K., A.D., R.C., B.J., C.E.L., D.G., L.P., R.D.S.; experimental studies, Y.H., B.J., V.P., D.G., R.D.S.; statistical analysis, H.I.S., S.L., H.B., B.C., R.D.S.; and manuscript editing, H.I.S., Y.H., A.D., C.D.P., B.J., V.P., J.P., L.V., L.P., S.L., B.C., R.D.S.

Conflicts of interest are listed at the end of this article.

See also the editorial by Haller in this issue.

and Centre Hospitalier Universitaire de Liège, Liège, Belgium) (*ClinicalTrials.gov* identifier NCT00577954). Investigators at these centers and in the United States established the Neuroimaging for Coma Emergence and Recovery (known as NICER) Consortium to map changes in brain structure and function in patients who are unconscious after severe neurologic injury (CA, brain trauma, and stroke) and to determine the relationship between such changes and long-term functional recovery and outcome; additional details on this project have been provided elsewhere (11,20,21). Clinical and structural MR imaging data on 20 of the patients included in the current study have been reported elsewhere (11).

This study was approved by the institutional review board at participating centers. To be included in this study, patients had to meet the following criteria: CA documented in the preceding 2 weeks, coma defined as inability to follow commands not attributed to sedation or aphasia, admission to the intensive care unit, mechanical ventilation, brain MR images obtained less than 28 days after CA, and a brain-imaging protocol that included a blood oxygen level–dependent sequence. Patients were excluded if there was any neurodevelopmental, neurologic, or psychiatric disorder that preceded CA. The study did not require any specific algorithm for temperature management, sedation, or any other aspect of critical care, all of which were at the discretion of providers in participating centers. MR imaging was not performed in patients who had rapidly evolving neurologic, circulatory, or respiratory instability, or if there was any other factor that precluded safe transport and MR imaging.

Data collected included patient demographics, etiologic cause of CA, first detected cardiac rhythm, time to return of spontaneous circulation, neurologic examination (Glasgow coma scale, pupillary light reflex, corneal reflex, motor deficits), temperature management, and use of sedation. The principal outcome was a dichotomized cerebral performance category (22) score evaluated 12 months after CA. The cerebral performance category is an outcome measure extensively validated in patients with CA that describes five levels of functional ability: 1, good cerebral performance (ie, alert, able to work); 2, moderate disability (ie, conscious, independent in most activities of daily living); 3, severe disability (ie, conscious but dependent in most activities of daily living); 4, coma or vegetative state; and 5, brain death. Patients with a cerebral performance category score of 1–2 were classified as having a favorable outcome (FO) and those with a cerebral performance category score of 3–5 were classified as having an unfavorable outcome.

The control group consisted of 48 age-matched healthy volunteers recruited from the community who had no history of neurologic or psychiatric disorder and who were not taking psychoactive medications.

MR Imaging Data Acquisition

Patients were accompanied to the imaging suite by an intensive care unit provider and had continuous monitoring of physiologic variables during MR imaging and associated transport. Sedation was administered by the intensive care unit team as needed to limit movement during the MR examination. Imaging of control participants was accomplished in a semidark and quiet environment; these control participants were instructed to close their eyes and think about nothing in particular during the resting-state functional MR imaging sequence.

Structural and functional MR imaging was performed on 3-T MR imagers at the three sites. Pulse sequences included a three-dimensional T1-weighted sequence, fluid-attenuated inversion recovery (FLAIR), and diffusion-weighted imaging (DWI). Functional T2*-weighted blood oxygen level–dependent images at resting-state functional MR imaging were acquired by using two-dimensional gradient-echo echo-planar imaging. MR imagers and image acquisition parameters varied according to site and are presented here.

Centre Hospitalier Universitaire de Liège.—Tim Trio imager (Siemens Medical Solutions, Erlangen, Germany). T1-weighted imaging: repetition time msec/echo time msec, 2300/2; voxel size, 1 × 1 × 1.2 mm. Resting-state functional MR imaging: 2000/30; voxel size, 3–3.4 × 3–3.4 × 3.75 mm; 300 volumes. FLAIR sequence: 6000/388; inversion recovery, 2100 msec; voxel size, 0.98 × 0.98 × 1 mm. DWI: 5700/87; voxel size, 1.79 × 1.79 × 3 mm. DWI for one participant was performed with slightly different parameters: 6000/75; voxel size, 0.89 × 0.89 × 3 mm.

Centre Hospitalier Universitaire de Clermont Ferrand.—Discovery MR750 imager (GE Healthcare, Waukesha, Wis). T1-weighted imaging: 8164/3.18; voxel size, 1 × 1 × 1 mm. Resting-state functional MR imaging: 2500/26; voxel size, 3.75 × 3.75 × 4 mm; 150 volumes. FLAIR sequence: 11000/150; inversion recovery, 2350 msec; voxel size, 0.47 × 0.47 × 3 mm. DWI: 4800/86.5–87.5, voxel size, 1.09 × 1.09 × 4 mm.

Groupe Hospitalier Pitié-Salpêtrière.—Signa HDxt imager (GE Healthcare). T1-weighted imaging: 7100–7336/3.09–3.11; voxel size, 0.49 × 0.49 × 1.2 mm. Resting-state functional MR imaging: 2400–3500/25–30; voxel size, 2.19–3.4 × 2.19–3.4 × 3–5 mm; 69–200 volumes. FLAIR sequence: 9000/150; inversion recovery, 2250; voxel size, 0.47 × 0.47 × 3 mm. DWI: 7000/61–71; voxel size, 1.09 × 1.09 × 5 mm.

The same imaging parameters were used for patients and control participants at each site.

Image Processing

Brain MR images were reviewed by a board-certified neuroradiologist (H.I.S., with 6 years of postfellowship experience) to evaluate for structural abnormalities. Participants with any evidence of territorial stroke of any age, intracranial hemorrhage, or intracranial mass lesions were excluded; in addition, any subject with head motion greater than 2 mm across the imaging session was excluded.

MR imaging morphologic analysis was accomplished by using two validated scores on the basis of a visual rating (23,24). In the system proposed by Hirsch et al (24), developed in a similar population with CA, the anatomic location and degree of signal abnormality

on FLAIR images and DWI sequences is rated from 0 (normal) to 4 (severe), and composite tissue signal change is then calculated in cortical, basal ganglia and thalamus, brainstem, and cerebellar structures (24). The sum of scores in cortical, basal ganglia, and all structures is referred to as the cortex, deep gray nuclei, and overall score, respectively. The sum or all scores recorded by using FLAIR and DWI is known as the DWI and FLAIR score, respectively (24). The second scoring system used was the Fazekas scale (23), which has been extensively validated to classify patients with small-vessel ischemic disease (25), and which we applied to FLAIR images. The Fazekas scale grades the magnitude of periventricular and deep white matter hyperintense areas on T2-weighted or FLAIR images from 0 (no lesion) to 3 (irregular periventricular signal extending into the deep white matter for periventricular white matter, or large confluent areas for deep white matter) (23).

Functional images were processed by using statistical parametric mapping (SPM version 8; Wellcome Trust, London, England) implemented in Matlab version R2011a (Mathworks, Natick, Mass). The first 10 volumes of resting-state functional MR imaging were discarded to allow for equilibrium. Section timing correction and motion correction were performed. The ART-repair toolbox in SPM was used with default parameters to repair functional MR imaging sections and volumes with significant artifact related to motion and global signal variance. T1-weighted images and functional MR images were coregistered for each participant and normalized to Montreal Neurological Institute space at 2-mm resolution. T1-weighted images were segmented into gray matter, white matter, and cerebrospinal fluid. These segmentation masks were eroded and binarized and white matter and cerebrospinal fluid regions of interest were created, which were used for physiologic nuisance removal of detrended functional MR images by using the anatomic component-based noise correction method (CompCor; 26). The nuisance-regressed functional MR image was bandpass filtered at 0.1–0.01 Hz and spatially smoothed by using a Gaussian kernel with full width at half maximum of 6 mm. Mean root mean square values for volume-to-volume head motion were calculated and compared between the control and anoxia groups.

Functional Connectivity Measurement and Statistical Analysis

A set of 77 network-grouped seeds were generated by using independent component analysis in a previously collected data set of healthy volunteers (27) via selection of the center of mass for each independent cluster identified on independent component analysis maps. From this set, seeds from four networks of interest were used: the dorsal attention network (DAN; 12 seeds), the default-mode network (DMN; 13 seeds), the executive control network (ECN; eight seeds), and the salience network (SN; seven seeds). These four networks were selected because they are well characterized in terms of their topography and are associated behavioral and cognitive phenotype of higher order brain function (16); in addition, these networks contribute most consistently to intersubject differences in connectivity (28). Time-dependent blood oxygen level–dependent fluctuations of each seed were extracted for each participant, and Pearson correlation coefficient was computed across all seed pairs. The resultant connectivity matrices were *z*-score normalized. Intrinsic within-network connectivity was expressed as the mean correlation of all seeds inside each network, and extrinsic between-network connectivity was expressed as the mean correlation between all seeds in network pairs (DMN-DAN, DMN-SN, DMN-ECN, DAN-SN, DAN-ECN, SN-ECN).

Data are expressed as means and standard deviation unless otherwise specified. Study participants were classified as follows for group comparisons: control participants, patients, patients with FO, and patients with unfavorable outcomes. Fisher exact test was used to compare categorical variables and Mann-Whitney *U* test was used for nonnormally distributed continuous variables. Between-group comparisons of within-network connectivity and between-network connectivity were adjusted in a multivariable model that included age, sex, and whether or not participants underwent sedation. Strength of the association between connectivity, structural measures, and the principal outcome was determined with the help of a multiple logistic regression model that adjusted for age, sex, and sedation status.

Classification accuracy of functional connectivity and structural measures was assessed by plotting receiver operating characteristic curves. Of the structural classifiers considered (23,24), overall DWI and overall FLAIR scores had the highest predictive accuracy and were therefore compared with the most discriminative resting state functional MR imaging classifiers, which were DMN within-network connectivity and DMN-SN internetwork connectivity. Correction for multiple comparisons was performed by dividing the error rate by the number of tests performed.

Results

Study Subjects and Outcome

Between July 2007 and October 2013, 46 patients with CA and 48 healthy age-matched control participants (mean age, 40.85 years ± 16.71; 22 men) were enrolled in three centers as follows: Paris, 33 patients and 17 control participants; Clermont-Ferrand, six patients and five control participants; and Liège, seven patients and 26 control participants. After CA, patients underwent MR imaging at mean 12.57 days ± 5.65. At 12 months, 11 patients (23.9%) had an FO (cerebral performance category score, 1–2) and 35 patients (76.1%) had an unfavorable outcome (cerebral performance category score, 3–5). Significant differences between outcome groups were age (FO group younger, $P = .025$), presenting with rhythm of ventricular fibrillation (more common in the FO group, $P = .038$), and out-of-hospital CA (more frequent in the FO group, $P = .044$). Patient characteristics are detailed in Table 1.

Structural MR Imaging Analysis and Motion

Brain MR imaging morphologic ratings are provided in Table 2. FLAIR and DWI scores were significantly higher in the patients with an unfavorable outcome compared with the patients with FO in all regions. However, the Fazekas scores were not different between groups. There was no statistically significant difference in head motion root mean square values between the control (root mean square value, 0.12) and anoxia (root mean square value, 0.08) groups ($P = .49$).

Functional Connectivity

Representative resting-state blood oxygen level–dependent maps in a control participant and in a patient with FO and unfavorable outcome are shown in Figure 1.

Patients versus control participants.—Connectivity matrices that demonstrate within-network connectivity and between-network connectivity in patients and control participants are shown in Figure 2a and 2b. Mean within-network connectivity values in patients were reduced in all networks (Fig 3), but after correction for multiple comparisons this difference remained significant only for the DMN ($P = .002$). Between-network connectivity (ie, the anticorrelation) was also reduced in patients versus control participants (Fig 4); the anticorrelation of SN-DMN and SN-ECN were significantly lower in patients compared with control participants ($P < .001$ and .02, respectively).

Patients with favorable versus unfavorable outcome.—Connectivity matrices showing within-network connectivity and between-network connectivity in patients with FO and patients with unfavorable outcome are provided in Figure 2c and 2d. Within-network connectivity was higher in all networks of patients with FO but only DMN remained significant after correction ($P = .002$; Fig 3). Between-network connectivity (ie, the anticorrelation) of DMN-SN and of ECN-SN were significantly higher in the FO group after correction ($P < .001$ and .002, respectively; Fig 4). The higher within-network connectivity in the DMN in patients with FO remained significant after adjusting for age, sex, and sedation status ($P = .002$). Similarly, the higher between-network connectivity of DMN-SN and of ECN-SN in patients with FO remained significant after this adjustment ($P < .001$ and $P = .02$, respectively).

Classification accuracy.—Receiver operating characteristic curves for prediction of 1-year functional outcome were plotted by using structural and functional connectivity MR imaging measures (Fig 5). Between-network DMN-SN connectivity (ie, the anticorrelation) was the most accurate predictor with an area under the curve of 0.88, higher than intrinsic DMN connectivity or composite DWI or FLAIR scores (respective areas under the curve of 0.73, 0.71 and 0.74).

Table 1

Clinical Characteristics of Patients Enrolled in the Study

Parameter	All Participants	FO	Unfavorable Outcome	*P* Value
No. of subjects	46	11	35	
Mean age (y)	49.46 (17.19)	38.09 (18.66)	53.03 (15.28)	.025
No. of men	32 (69.56)	9 (81.81)	23 (65.71)	.46
No. of out-of-hospital CAs	35 (76.08)	11 (100)	24 (68.57)	.044
No. with ventricular fibrillation	20 (43.47)	8 (72.72)	12 (34.28)	.038
Mean time to ROSC (min)	34.7 (26.8)	43 (45)	32.1 (17.7)	.61
No. with therapeutic hypothermia	39 (84.78)	8 (72.72)	31 (88.57)	.14
Median GCS*	5.6 (3–9)	6 (3–9)	5 (3–7)	.37
No. with presence of pupillary reflex	34 (73.9)	8 (72.7)	26 (74.2)	1.00
Mean time from CA to MR imaging (d)†	12.57 ± 5.65	12.55 ± 6.47	12.57 ± 5.47	.99
No. who underwent sedation during MR imaging	14 (30.43)	4 (36.36)	10 (28.57)	.71
Mean length of stay in ICU (d) †	19.55 ± 10.67	19.09 ± 10.49	19.7 ± 10.88	.91

Note.—Unless otherwise indicated, data in parentheses are percentages. ROSC = return of spontaneous circulation, GCS = Glasgow coma scale, ICU = intensive care unit.

* Data in parentheses are range.

† Data are ± standard deviation.

Discussion

The results demonstrate that abnormalities in long-range connectivity occur within and between canonical brain networks in the acute phase of anoxic brain injury, and these abnormalities are associated with long-term functional outcome. The link between functional connectivity and outcome was observed even after adjustment in multivariable models and improved classification compared with postanoxic structural changes appreciated by using morphologic acquisition sequences (FLAIR and DWI). Connectivity differences between groups were observed in a graded fashion from control participants to FO to unfavorable outcome (Figs 2, 3), a pattern that has biologic plausibility and supports our hypothesis of large-scale network dysfunction in anoxic brain injury. Taken together with our earlier work that identified structural damage in central white matter tracts as a predictive variable (11,20) and impaired DMN activity (12) in CA survivors, these data suggest that anatomic and functional disconnection occurs early after CA and could represent a biomarker of recovery potential.

The relationship between the acute phase of CA, anoxic brain injury, and resting-state functional MR imaging network connectivity has been considered in other studies (29–31). By using a graph theoretical approach to resting-state functional MR imaging data in 17 coma patients (of whom 12 presented after CA, MR images obtained at 3–16

Table 2

Brain MR Imaging Morphologic Scores

Parameter	Patients with FO	Patients with Unfavorable Outcome	*P* Value
Overall score	12.8 ± 8.2	32.5 ± 18.4	.0001
Cortex score	8.9 ± 4.9	15.8 ± 8.7	.0025
DGN score	2.9 ± 3.9	9.2 ± 6.3	.0005
Cortexv and DGN score	11.8 ± 7.7	24.9 ± 13.7	.0003
DWI score	7.3 ± 4.6	17.9 ± 11.3	.0001
FLAIR score	5.5 ± 4.1	14.6 ± 8.5	.0001
Fazekas score			
PVWM	1.18 ± 0.6	1.2 ± 0.7	.83
DWM	0.90 ± 0.5	0.94 ± 0.8	.87
Total	2.09 ± 1.0	2.17 ± 1.4	.84

Note.—Data are ± standard deviation. DGN = deep gray nuclei, DWM = deep white matter, PVWM = periventricular white matter.

Figure 1

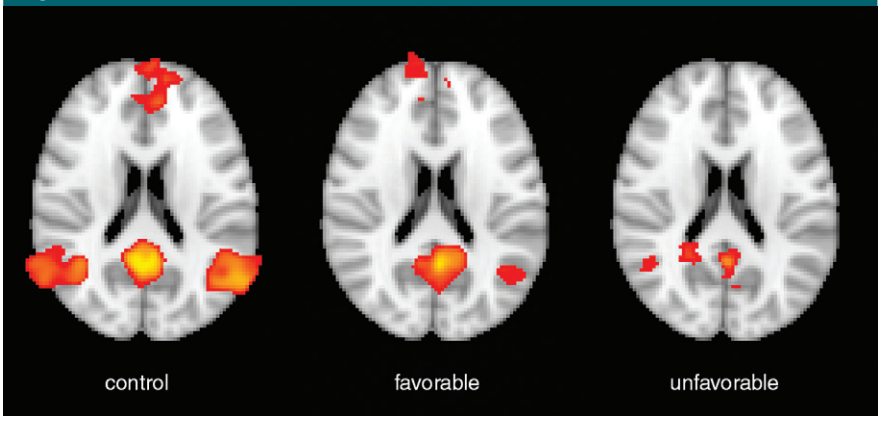

Figure 1: Representative DMN resting blood oxygen level–dependent maps in a control participant (left), patient with FO (middle), and a patient with an unfavorable outcome (right) overlaid onto axial standard Montreal Neurological Institute template (*z* score, 46). The posterior cingulate (MNI: 45, 37, 49) was seeded and voxels with Pearson correlations greater than 0.6 are shown in red–yellow.

days), Achard et al (29) found that although global network measures were largely the same between patients and healthy control participants, significant differences were reported in properties of individual cortical nodes, with highly connected nodes (ie, hubs) in control participants noted to be nonhubs in patients, and vice versa. Of note, this study did not examine specific networks, and therefore the relationship between network characteristics and outcome was not determined. In 13 patients studied 1–6 days after CA, Norton et al (31) found that DMN activation and connectivity was preserved in the two patients who regained consciousness at 3 months, whereas DMN activity could not be identified in the 11 patients who remained unconscious. In a study of 17 patients who underwent resting-state functional MR imaging 4–7 days after CA, Koenig et al (30) reported decreased DMN connectivity compared with healthy control participants and an association between cerebral performance category at discharge and precuneus and posterior cingulate cortex connectivity. In a separate study of patients with trauma and anoxic coma (14 and 13 patients, respectively), PCC connectivity with brain areas that normal synchronized with the PCC was significantly disrupted (32). Similarly, a recent coordinate-based meta-analysis (12) of resting-state neuroimaging studies acquired in patients with disorders of consciousness demonstrated significantly reduced activity in nodes of the DMN. Here, we extended these previous findings via an analysis of higher-order intrinsic brain networks (DMN, DAN, ECN, SN) that considers both intra-network (ie, within-network) connectivity and inter-network (ie, between-network) connectivity properties; moreover, we evaluated functional outcome at 1 year in survivors. Our finding of decreased functional connectivity in the DMN in patients with CA compared with control participants is consistent with previous work (30,31,33). In addition, we demonstrated diminished functional connectivity in two other intrinsic networks (SN and ECN) and loss of normal SN-DMN and SN-ECN anticorrelations, which was consistently observed in healthy participants. When patients with unfavorable outcome were compared with those with FO, they had a reduction in DMN connectivity and a loss of SN-DMN and SN-ECN anticorrelation that remained significant even after adjustment in a multivariable analysis.

The DMN is a distributed system with nodes in the precuneus, posterior cingulate cortex, thalamus, and medial prefrontal cortex; whereas activation within the DMN has not been consistently mapped to a specific function, deactivation of this system is reliably associated with engagement in goal-oriented tasks (34). Abnormalities of the DMN have been detected in a range of neurologic and psychiatric disorders and in patients with disorders of consciousness (33,35). The SN, in which the key nodes are the anterior insula, presupplementary motor area, and dorsal anterior cingulate cortex, integrates contextually important sensory, visceral, autonomic, and attention inputs to generate appropriate behavioral responses (36,37). Activity in the SN is anticorrelated with the DMN and the ECN, and it has been proposed that one of the SN nodes, the dorsal anterior insular cortex, is a critical hub controlling activation or deactivation of other functional networks (38). In a study of patients with traumatic brain injury,

Figure 2

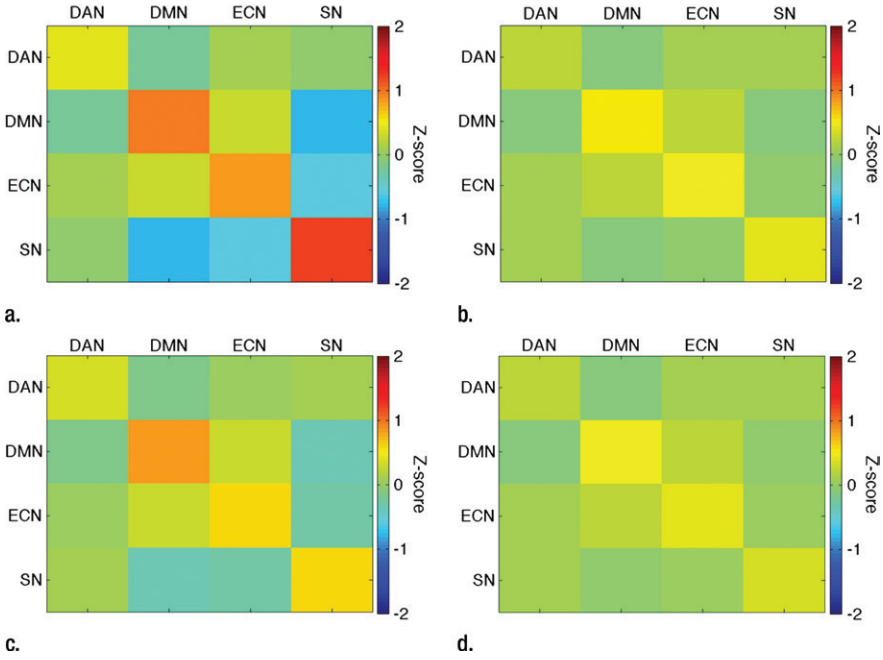

Figure 2: Group connectivity matrices. Connectivity matrices of **(a)** control, **(b)** anoxia, **(c)** FO, and **(d)** unfavorable outcome groups. The *z* score normalized mean connectivity is shown within (diagonal of matrix) and between (off-diagonal of matrix) networks. Positive values (toward red) denote positive correlations, negative values (toward blue) denote negative correlations, and values near zero (green) denote absence of correlation.

Figure 3

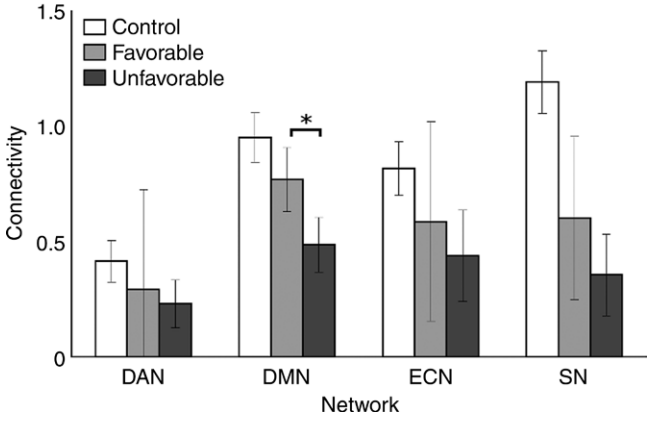

Figure 3: Box-and-whisker plot shows connectivity strength within networks. Bars represent *z* score normalized mean connectivity values in the canonical networks of interest, comparing control participants, patients with CA with FO, and those with unfavorable outcome. Error bars denote twice the standard error of the mean. * Significant differences in group means.

the amount of white matter damage in tracts that connect the anterior insula to the presupplementary motor area and to anterior cingulate cortex predicted DMN function (39). We found that the SN-DMN and SN-ECN anticorrelation observed in healthy control participants was significantly reduced in patients with CA; furthermore, patients with an unfavorable outcome had significantly reduced SN-DMN and SN-ECN anticorrelated activity when compared with patients with FO. These findings are congruent with a recent study from members of our group in which partial preservation of between-network anticorrelations clearly differentiated between patients who remained in a vegetative or minimally conscious state from patients who had higher levels of consciousness (35); however, distinct from this latter investigation, which was performed in the chronic phase after brain injury, our study examined the acute phase when decisions regarding prognostication and therapeutic intervention might have greater effect. In another study (40) conducted in patients with hemorrhagic stroke, loss of consciousness was linked to decreased anticorrelation between the DMN and the so-called task-positive network (which includes nodes in the SN). Collectively, these observations support a model in which connectivity of the SN and its ability to regulate other networks could be a determinant of coma emergence, and possibly a target for therapeutic intervention. Certainly the role of the SN and its substructures as major hubs which drive neurologic function and disease states deserves investigation (41).

The results presented here of early dysfunction involving multiple canonical networks, and the link between these acute changes and long-term post-CA functional outcome, provide a methodologic and conceptual framework for future studies to be conducted in this population. However, several limitations must be recognized. First, sedation was administered in a subset of patients to limit motion artifact and to enhance patient safety during MR imaging. Sedative and anesthetic agents have distinct effects on synaptic transmission, cerebral metabolism, and blood flow, which may modify blood oxygen level–dependent signal responses that are the basis for functional MR imaging (42). Moreover, recent work indicated that resting functional connectivity measures may change in varying degrees during sedation and general anesthesia (43). The use of sedation may have confounded observed connectivity differences between patients with CA and healthy

Figure 4

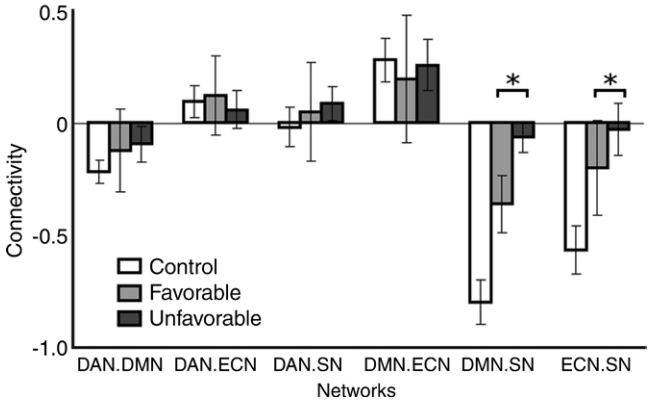

Figure 4: Box-and-whisker plot shows connectivity strength between networks. Bars represent *z* score normalized mean connectivity strength between networks of interest, comparing control participants, patients with CA with FO, and those with unfavorable outcome. Error bars denote twice the standard error of the mean. Significant differences in group means are denoted by asterisks. *DAN.DMN* = DAN–DMN connectivity; *DAN.ECN* = DAN–ECN connectivity; *DAN.SN* = DAN–SN connectivity; *DMN.ECN* = DMN–ECN connectivity; *DMN.SN* = DMN–SN connectivity, *ECN.SN* = ECN–SN connectivity.

Figure 5

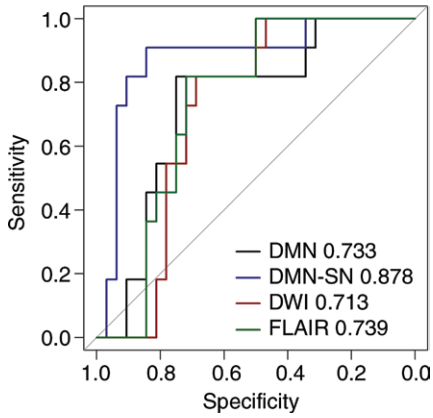

Figure 5: Leave-one-out cross-validated receiver operating characteristic curves for the prediction of 1-year functional outcome after CA. Shown are curves for the two most predictive functional imaging classifiers among those considered (DMN and DMN-SN), and the curves for the most predictive structural imaging classifiers among those considered (DWI, FLAIR). Areas under the curves are shown for each metric in the inset.

control participants (none of whom received sedation); however, there was no difference in the proportion of patients who underwent sedation when FO and unfavorable outcome patient groups were compared, and the use of sedatives was adjusted for the multivariable model, hence it is unlikely that connectivity differences noted between those groups would be significantly confounded in this manner. A second potential limitation relates to reliability of the blood oxygen level–dependent signal in the post-CA setting. Whereas impaired neurovascular coupling has been reported in experimental models of global cerebral ischemia (44), evidence of such an effect in humans is limited. Research is needed to explore this issue as a potential confounding variable in functional MR imaging inference. A third limitation is that the small sample size and heterogeneity precluded the establishment of a clinically tractable prognostic model. However, this was not the primary objective of our study, and longitudinal investigations conducted in appropriately powered cohorts are needed to confirm these findings and validate them in prediction systems that could support clinical decision making.

In summary, when conducted in the acute phase after CA, MR imaging shows that preservation of resting-state functional connectivity within the DMN and between the default mode and SNs are linked with a higher likelihood of 1-year functional recovery. The biologic significance of these results, and their validity in the clinical setting, merit further investigation.

Disclosures of Conflicts of Interest: H.I.S. disclosed no relevant relationships. **Y.H.** disclosed no relevant relationships. **S.L.** disclosed no relevant relationships. **J.K.** disclosed no relevant relationships. **A.D.** disclosed no relevant relationships. **C.D.P.** disclosed no relevant relationships. **R.C.** disclosed no relevant relationships. **B.J.** disclosed no relevant relationships. **H.B.** disclosed no relevant relationships. **V.P.** disclosed no relevant relationships. **J.P.** Activities related to the present article: disclosed no relevant relationships. Activities not related to the present article: disclosed grants from the F.M. Kirby Research Center for Functional Brain Imaging, which receives research support from Philips Healthcare. Other relationships: disclosed no relevant relationships. **C.E.L.** Activities related to the present article: disclosed no relevant relationships. Activities not related to the present article: reports personal fees from Bayer Healthcare, personal fees from MSD, personal fees from ThermoFisher, outside the submitted work. Other relationships: disclosed no relevant relationships. **D.G.** disclosed no relevant relationships. **L.V.** disclosed no relevant relationships. **L.P.** Activities related to the present article: disclosed no relevant relationships. Activities not related to the present article: disclosed patent issued for ex vivo method for quantifying brain injuries. Other relationships: disclosed no relevant relationships. **S.L.** disclosed no relevant relationships. **B.C.** disclosed no relevant relationships. **R.D.S.** disclosed no relevant relationships.

References

1. Mozaffarian D, Benjamin EJ, Go AS, et al. Heart disease and stroke statistics--2015 update: a report from the American Heart Association. Circulation 2015;131(4):e29–e322.
2. Fugate JE, Moore SA, Knopman DS, et al. Cognitive outcomes of patients undergoing therapeutic hypothermia after cardiac arrest. Neurology 2013;81(1):40–45.
3. Hofmeijer J, Beernink TM, Bosch FH, Beishuizen A, Tjepkema-Cloostermans MC, van Putten MJ. Early EEG contributes to multimodal outcome prediction of postanoxic coma. Neurology 2015;85(2):137–143.
4. Rossetti AO, Oddo M, Logroscino G, Kaplan PW. Prognostication after cardiac arrest and hypothermia: a prospective study. Ann Neurol 2010;67(3):301–307.
5. Stevens RD, Sutter R. Prognosis in severe brain injury. Crit Care Med 2013;41(4):1104–1123.
6. Kamps MJ, Horn J, Oddo M, et al. Prognostication of neurologic outcome in cardiac arrest patients after mild therapeu-

tic hypothermia: a meta-analysis of the current literature. Intensive Care Med 2013;39(10):1671–1682.

7. Bouwes A, Binnekade JM, Kuiper MA, et al. Prognosis of coma after therapeutic hypothermia: a prospective cohort study. Ann Neurol 2012;71(2):206–212.
8. Harris NG, Zilkha E, Houseman J, Symms MR, Obrenovitch TP, Williams SR. The relationship between the apparent diffusion coefficient measured by magnetic resonance imaging, anoxic depolarization, and glutamate efflux during experimental cerebral ischemia. J Cereb Blood Flow Metab 2000;20(1):28–36.
9. Mlynash M, Campbell DM, Leproust EM, et al. Temporal and spatial profile of brain diffusion-weighted MRI after cardiac arrest. Stroke 2010;41(8):1665–1672.
10. Wijman CA, Mlynash M, Caulfield AF, et al. Prognostic value of brain diffusion-weighted imaging after cardiac arrest. Ann Neurol 2009;65(4):394–402.
11. Luyt CE, Galanaud D, Perlbarg V, et al. Diffusion tensor imaging to predict long-term outcome after cardiac arrest: a bicentric pilot study. Anesthesiology 2012;117(6):1311–1321.
12. Hannawi Y, Lindquist MA, Caffo BS, Sair HI, Stevens RD. Resting brain activity in disorders of consciousness: a systematic review and meta-analysis. Neurology 2015;84(12):1272–1280.
13. Vincent JL, Patel GH, Fox MD, et al. Intrinsic functional architecture in the anaesthetized monkey brain. Nature 2007;447(7140):83–86.
14. Damoiseaux JS, Rombouts SA, Barkhof F, et al. Consistent resting-state networks across healthy subjects. Proc Natl Acad Sci U S A 2006;103(37):13848–13853.
15. Fox MD, Snyder AZ, Vincent JL, Corbetta M, Van Essen DC, Raichle ME. The human brain is intrinsically organized into dynamic, anticorrelated functional networks. Proc Natl Acad Sci U S A 2005;102(27):9673–9678.
16. Pievani M, de Haan W, Wu T, Seeley WW, Frisoni GB. Functional network disruption in the degenerative dementias. Lancet Neurol 2011;10(9):829–843.
17. Cao M, Wang JH, Dai ZJ, et al. Topological organization of the human brain functional connectome across the lifespan. Dev Cogn Neurosci 2014;7:76–93.
18. Seeley WW, Crawford RK, Zhou J, Miller BL, Greicius MD. Neurodegenerative diseases target large-scale human brain networks. Neuron 2009;62(1):42–52.
19. Martino M, Magioncalda P, Huang Z, et al. Contrasting variability patterns in the default mode and sensorimotor networks balance in bipolar depression and mania. Proc Natl Acad Sci U S A 2016;113(17):4824–4829.
20. van der Eerden AW, Khalilzadeh O, Perlbarg V, et al. White matter changes in comatose survivors of anoxic ischemic encephalopathy and traumatic brain injury: comparative diffusion-tensor imaging study. Radiology 2014;270(2):506–516.
21. Galanaud D, Perlbarg V, Gupta R, et al. Assessment of white matter injury and outcome in severe brain trauma: a prospective multicenter cohort. Anesthesiology 2012;117(6):1300–1310.
22. Brain Resuscitation Clinical Trial I Study Group. Randomized clinical study of thiopental loading in comatose survivors of cardiac arrest. N Engl J Med 1986;314(7):397–403.
23. Fazekas F, Chawluk JB, Alavi A, Hurtig HI, Zimmerman RA. MR signal abnormalities at 1.5 T in Alzheimer's dementia and normal aging. AJR Am J Roentgenol 1987;149(2):351–356.
24. Hirsch KG, Mlynash M, Jansen S, et al. Prognostic value of a qualitative brain MRI scoring system after cardiac arrest. J Neuroimaging 2015;25(3):430–437.
25. Prins ND, Scheltens P. White matter hyperintensities, cognitive impairment and dementia: an update. Nat Rev Neurol 2015;11(3):157–165.
26. Behzadi Y, Restom K, Liau J, Liu TT. A component based noise correction method (CompCor) for BOLD and perfusion based fMRI. Neuroimage 2007;37(1):90–101.
27. Landman BA, Huang AJ, Gifford A, et al. Multi-parametric neuroimaging reproducibility: a 3-T resource study. Neuroimage 2011;54(4):2854–2866.
28. Airan RD, Vogelstein JT, Pillai JJ, Caffo B, Pekar JJ, Sair HI. Factors affecting characterization and localization of interindividual differences in functional connectivity using MRI. Hum Brain Mapp 2016;37(5):1986–1997.
29. Achard S, Delon-Martin C, Vértes PE, et al. Hubs of brain functional networks are radically reorganized in comatose patients. Proc Natl Acad Sci U S A 2012;109(50):20608–20613.
30. Koenig MA, Holt JL, Ernst T, et al. MRI default mode network connectivity is associated with functional outcome after cardiopulmonary arrest. Neurocrit Care 2014;20(3):348–357.
31. Norton L, Hutchison RM, Young GB, Lee DH, Sharpe MD, Mirsattari SM. Disruptions of functional connectivity in the default mode network of comatose patients. Neurology 2012;78(3):175–181.
32. Silva S, de Pasquale F, Vuillaume C, et al. Disruption of posteromedial large-scale neural communication predicts recovery from coma. Neurology 2015;85(23):2036–2044.
33. Vanhaudenhuyse A, Noirhomme Q, Tshibanda LJ, et al. Default network connectivity reflects the level of consciousness in non-communicative brain-damaged patients. Brain 2010;133(Pt 1):161–171.
34. Fair DA, Cohen AL, Dosenbach NU, et al. The maturing architecture of the brain's default network. Proc Natl Acad Sci U S A 2008;105(10):4028–4032.
35. Di Perri C, Bahri MA, Amico E, et al. Neural correlates of consciousness in patients who have emerged from a minimally conscious state: a cross-sectional multimodal imaging study. Lancet Neurol 2016;15(8):830–842.
36. Seeley WW, Menon V, Schatzberg AF, et al. Dissociable intrinsic connectivity networks for salience processing and executive control. J Neurosci 2007;27(9):2349–2356.
37. Sridharan D, Levitin DJ, Menon V. A critical role for the right fronto-insular cortex in switching between central-executive and default-mode networks. Proc Natl Acad Sci U S A 2008;105(34):12569–12574.
38. Menon V, Uddin LQ. Saliency, switching, attention and control: a network model of insula function. Brain Struct Funct 2010;214(5-6):655–667.
39. Bonnelle V, Ham TE, Leech R, et al. Salience network integrity predicts default mode network function after traumatic brain injury. Proc Natl Acad Sci U S A 2012;109(12):4690–4695.
40. Mikell CB, Banks GP, Frey HP, et al. Frontal networks associated with command following after hemorrhagic stroke. Stroke 2015;46(1):49–57.
41. Uddin LQ. Salience processing and insular cortical function and dysfunction. Nat Rev Neurosci 2015;16(1):55–61.
42. Qiu M, Ramani R, Swetye M, Rajeevan N, Constable RT. Anesthetic effects on regional CBF, BOLD, and the coupling between task-induced changes in CBF and BOLD: an fMRI study in normal human subjects. Magn Reson Med 2008;60(4):987–996.
43. Boveroux P, Vanhaudenhuyse A, Bruno MA, et al. Breakdown of within- and between-network resting state functional magnetic resonance imaging connectivity during propofol-induced loss of consciousness. Anesthesiology 2010;113(5):1038–1053.
44. Baker WB, Sun Z, Hiraki T, et al. Neurovascular coupling varies with level of global cerebral ischemia in a rat model. J Cereb Blood Flow Metab 2013;33(1):97–105.